



Recovery of Metals from Copper Smelting Slag Using Coke and Biochar

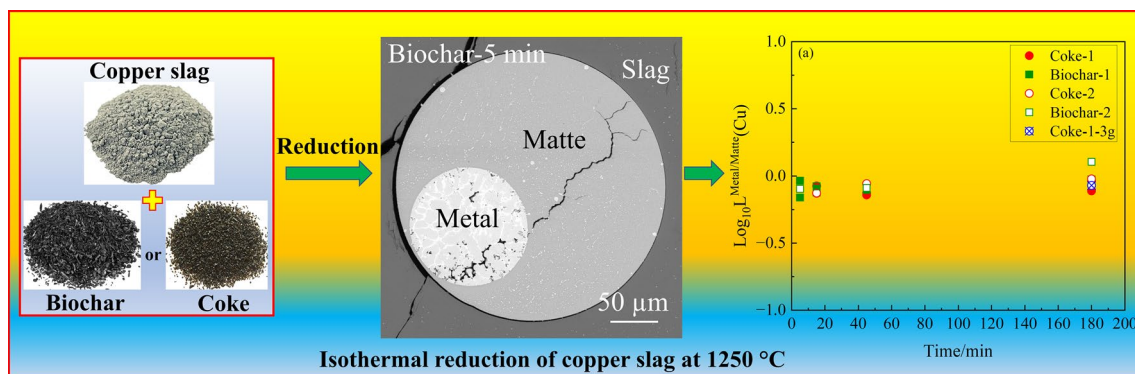
Min Chen^{1,4} · Dmitry Sukhomlinov¹ · Pekka Taskinen¹ · Joseph Hamuyuni² · Radoslaw M. Michallik³ · Mari Lindgren² · Ari Jokilaakso¹

Received: 5 November 2023 / Accepted: 10 January 2024 / Published online: 29 February 2024
© The Author(s) 2024

Abstract

With the purpose of recovering the metal values, in this study the copper slag was reduced by coke and biochar at 1250 °C in an argon gas atmosphere using the isothermal reduction/drop quenching technique. The phase compositions of metal, matte, and slag were determined using electron probe microanalysis (EPMA). The effects of reduction time and amount of reductant were investigated. The distribution of elements between metal/matte and slag was ascertained based on the elemental concentrations determined by EPMA. It was found that copper concentration in slag can be effectively decreased to approximately 0.4–0.6 wt% within 5 min by coke and biochar. Copper and nickel can also be successfully recovered into the copper alloy phase once settling has been accomplished.

Graphical Abstract



Keywords Circular economy · Resource efficiency · Hazardous materials · Reduction · Slag cleaning

The contributing editor for this article was Hongmin Zhu.

✉ Min Chen
min.chen@swerim.se

Dmitry Sukhomlinov
dmitry.sukhomlinov@aalto.fi

Pekka Taskinen
pekka.taskinen@aalto.fi

Joseph Hamuyuni
joseph.hamuyuni@mogroup.com

Radoslaw M. Michallik
radoslaw.michallik@gtk.fi

Mari Lindgren
mari.lindgren@mogroup.com

Ari Jokilaakso
ari.jokilaakso@aalto.fi

- 1 Department of Chemical and Metallurgical Engineering, School of Chemical Engineering, Aalto University, Kemistintie 1F, P.O. Box 16100, 00076 Aalto, Finland
- 2 Metso Research Center, Kuparitie 10, P.O. Box 69, 28101 Pori, Finland
- 3 Geological Survey of Finland, Vuorimiehentie 2, 02150 Espoo, Finland
- 4 Present Address: Process Metallurgy, Swerim AB, Aronstorpsvägen 1, Box 812, 97437 Luleå, Sweden

Introduction

With the continuously increasing demand for copper in equipment manufacturing, building construction, and infrastructure, it was estimated that global primary copper production would grow by 2.9% to approximately 22 million metric tons in 2022 which means the generation of 60–70 Mt pa of slag [1]. This is in addition to the forecasted major growth of copper demand as a result of the electrification of society and the utilization of renewable energy sources. Copper is mainly extracted from sulfide mineral ores through pyrometallurgical techniques [2, 3], among which more than 50% of annual output comes from Metso flash smelting technology [4]. The copper slag produced in flash smelting furnaces contains valuable metals (e.g., Cu, Co, Ni, and Zn) and heavy metals (Pb, As, and Sb) which require slag cleaning [1, 5, 6] before being landfilled. The cleaning of copper slag has attracted increasing attention due to the benefit of environmental protection and circular economy [7–12] but the use of slags in other areas is limited [1, 13].

The carbothermic reduction of copper slag is one of the efficient techniques for copper slag cleaning and recovery of its metal values [1]. Table 1 summarizes the recent studies [9, 11, 12, 14–29] on copper slag reduction using different reductants as carbon sources. In most

previous studies, the slag was slowly cooled after reduction [9, 11, 15, 16, 19, 20, 24, 27, 29]. The slow cooling of the reduced slag leads to the redistribution of elements between the phases, which means the metal concentrations in slag do not represent the situations at high temperatures. Moreover, the chemical analysis techniques used in most previous studies [9, 14–22] may cause inaccuracies in measuring the metal concentrations in slag and their distributions due to incomplete separation of metal and slag. The behaviors of elements in the carbothermic reduction of copper slag have not been systematically investigated. To determine the optimal operating conditions for copper slag cleaning, it is critical to understand the elemental distributions in copper slag reduction.

In this study, the effects of the reduction time and the amount of reductant on the distribution of elements between metal/matte and slag were investigated using high-temperature isothermal reduction followed by the drop quenching technique [30, 31]. The concentrations of metals in all phases were analyzed by EPMA. The present work helps to understand the behaviors of various elements in copper smelting slag cleaning using coke and biochar. The main motivation for the investigation was to find out the potential of biochar as a replacement for fossil coke as the reductant in the slag cleaning process.

Table 1 Recent studies on copper slag cleaning by carbothermic reduction

Carbon source	Temperature/°C	Cooling rate/(deg/min)	Analytical methods	Reference
Graphite	1300–1450	2	SEM–EDS, XRD, TG–DTA, and ICP–OES	[9]
Walnut shell char	900–1300	Not reported	SEM–EDS, TG, EPMA, XRD, and FTIR	[11]
Waste cooking oil	600–1300	Not reported	SEM–EDS, XRD, EPMA, and FTIR	[12]
Graphite	1500	Rapid quenching	XRD, SEM–EDS, and Chemical analysis	[14]
Coal	1100–1300	Cooled in N ₂	XRD, SEM–EDS, EPMA, and Chemical analysis	[15, 16]
Coal	1500	Rapid cooling in Ar	XRD, Chemical analysis	[17]
Anthracite	1500–1600	Not reported	XRD, Chemical analysis	[18]
Coal	1100–1300	Cooled in N ₂	XRF, XRD, EPMA, and Chemical analysis	[19]
Coke	1100–1300	Cooled in N ₂	XRD, XRF, SEM–EDS, Chemical analysis	[20]
Coke	1250–1480	Not reported	AAS and Chemical analysis	[21]
Anthracite	900–1300	Not reported	XRD, SEM–EDS, ICP–AES, FTIR, XPS	[22]
Biochar	25–1450	–	TG, XRD	[23]
Charcoal, Bamboo char, and Straw fiber	600–1300	Cooled in N ₂	SEM, TG, and XRD	[24]
Activated carbon	1400–1600	Not reported	XRD, XRF, EDS	[25]
Waste cooking oil	1230–1290	Not reported	AAS, SEM–EDS, and EPMA	[26]
Coal	1100–1300	Cooled in Ar	XRD, SEM–EDS, XRF	[27]
Graphite	25–1300	–	XRD, TG	[28]
Anthracite	1200	Cooled in air	XRD, SEM–EDS, and XPS	[29]

SEM scanning electron microscopy, *EDS* energy dispersive spectrometry, *XRD* X-ray diffraction analysis, *XRF* X-ray fluorescence analysis, *EPMA* electron probe microanalysis, *TG* thermogravimetric analysis, *DTA* differential thermal analysis, *FTIR* fourier transform infrared spectroscopy, *ICP* inductively coupled plasma spectroscopy, *AAS* atomic absorption spectrometry, *AES* atomic emission spectroscopy, *OES* optical emission spectrometry

Methodology

Thermodynamic Analysis of Carbothermic Reduction Reactions

To confirm the feasibility of the carbothermic reduction of copper slag at high temperatures, the possible reduction reactions of oxides in copper slag with solid carbon, as listed in reactions Eqs. 1–9, were analyzed using equilibrium calculations by MTDATA in open system mode by removing the gas phase from the system after each carbon addition step and equilibration. The ferric oxide in copper slag was expected to be reduced into wüstite and further dissolve in the copper before forming a solid iron alloy. The details of the initial slag compositions (see Table S1) and the boundary conditions used in the calculations are presented in the online Supplementary Material file.

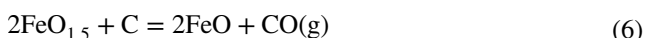


Figure 1 shows the calculated changes in slag and gas compositions as a function of the reduction degree. The lower content of $\text{FeO}_{1.5}$ in liquid oxide, shown as the X-axis in Fig. 1, represents a higher reduction degree. The equilibrium calculation was carried out stepwise in an open system where the formed gas phase was removed from the calculation prior to the following coke addition. The thermodynamic data for the computational equilibrium were retrieved from the *Mtox* and *SUB_SGTE* databases of MTDATA software [32]. The reduction generated two alloy phases so that LIQUID(1) was a sulfide matte and LIQUID(2) was a low-sulfur speiss-related alloy with high arsenic and iron content (see details in Fig. S1 and Fig. S2 of the online Supplementary Material file). For simplicity, the coke was assumed to be pure carbon.

Figure 1a indicates that the concentrations of copper, nickel, and arsenic in copper slag increase when the reduction has proceeded to some extent, due to the preferential reduction of $\text{FeO}_{1.5}$ to FeO . The calculated total mass of matte and alloy decrease and increase, respectively, with an increasing reduction degree, as shown in Fig. 1b. The predicted copper and iron concentrations in the copper alloy, as shown in Fig. 1c, remain almost constant when the $\text{FeO}_{1.5}$ in slag varies between 0.1 wt% and approximately 0.03 wt%. However, with the increase in reduction degree, the fractions of copper decrease and the iron fractions in the copper alloy increase simultaneously. Figure 1d shows that the amount of CO_2 generated in the gas phase decreases with an increasing reduction degree, whereas the concentration of CO in the gas phase displays the opposite increasing trend compared with CO_2 . The concentration of SO_2 in the gas phase drops dramatically at the very beginning of the reduction process. The calculation indicates that zinc preferentially evaporates into the gas phase.

Materials

The copper slag used in this study was provided by Metso Research Center, Pori, Finland. The chemical compositions of the copper matte-making slag are listed in Table 2 and the mineralogical cross-section and XRD pattern are shown in Fig. 2. The micrograph of the copper slag indicates that it mainly consisted of fayalite, magnetite, intergranular glass, and physically entrained copper matte. The fayalite and magnetite phases were also identified by XRD. However, the intergranular glass was not detected by XRD since it was amorphous.

Coke (Boliden Harjavalta) and biochar (Carbons Finland Oy, Kouvola, Finland) were used as reductants in the reduction experiments. The coke was crushed in an agate mortar from a particle size of 8–20 mm into smaller particles (< 1 mm) and the biochar was dried at 100 °C for 20 h to reach a moisture content of approximately 23 wt%, which was calculated by weighing the biochar before and after drying. The compositions of coke and biochar and the amount of reductant with the different stoichiometric amounts for each experiment used in this study are displayed in Table 3. The specific surface area of biochar reported by the supplier was > 500 m²/g. The particle size of 500–1000 μm for the pretreated coke and biochar was selected to represent the typical particle size in industrial practice. Cone-shaped fused silica crucibles (> 99.998%, Finnish SpecialGlass Oy, Espoo, Finland) were used for the experiments.

Experimental Setup and Procedures

The experiments on the high-temperature isothermal reduction of copper slag were conducted in a vertical Lenton tube

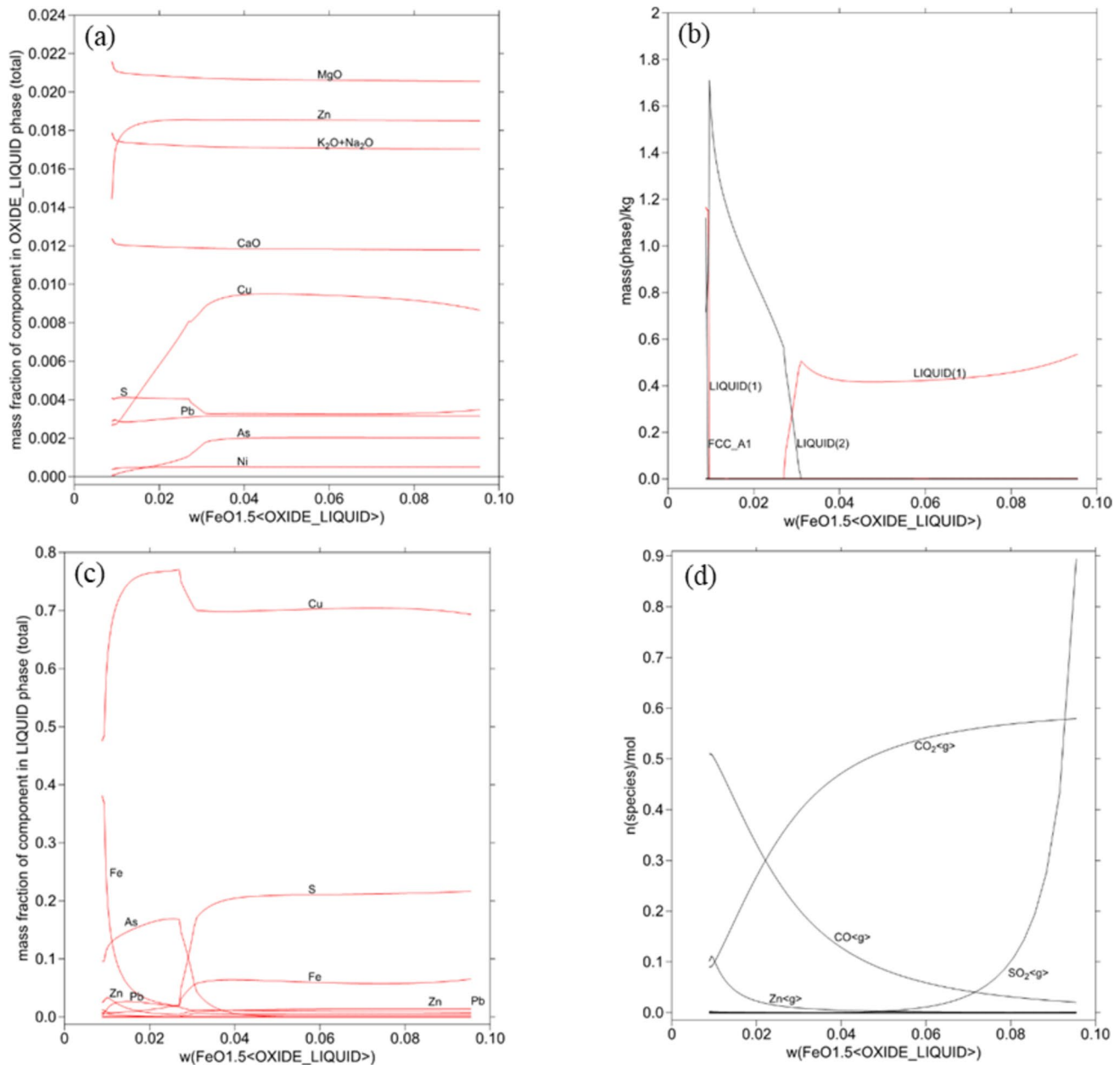


Fig. 1 Development of the equilibrium in coke reduction of copper slag at 1250 °C: **a** composition of the minority components in the molten slag, **b** amounts of metallic reduction products, **c** average

composition of liquid alloy phases, and **d** outlet gas composition as a function of the ferric oxide ($\text{FeO}_{1.5}$) concentration of the slag

furnace (Lenton PTF 15/45/450, UK) heated using SiC heating elements, as described in detail in our previous studies [33–35]. Figure 3 shows a schematic diagram of the reduction furnace. The sample temperature was measured by a calibrated S-type Pt/Pt-10% Rh thermocouple placed on the top of the sample. In each experiment, approximately 1 g of copper slag was mixed manually with one or two stoichiometric amounts of coke/biochar before being placed into the silica crucible. The stoichiometric ratio of carbon was calculated based on the aim of reducing all metal oxides

of interest into pure metal. The mixing of copper slag and reductants was only conducted by the initial manual mixing, without employing a lance to blow gas into the molten slag.

The experiment was started by introducing the samples into the cold zone of the furnace using Kanthal A1 wire before charging pure Ar (300 mL/min, 99.999 vol%, Woikoski Oy, Finland) into the furnace. The bottom of the furnace reaction tube was sealed using a rubber cork. After stabilizing the gas atmosphere for 15 min, the sample was lifted into the hot zone for reduction. The sample was then quenched in

Table 2 Chemical composition of industrial copper slag

Component	Method	Concentration/ wt%
Na	ICP	0.42
Mg	ICP	1.19
Al	ICP	2.14
K	ICP	0.89
Ca	ICP	0.81
Fe	ICP	38.30
Co	ICP	0.06
Ni	ICP	0.05
Cu	ICP	1.19
Zn	ICP	1.78
As	ICP	0.19
Sb	ICP	0.10
Pb	ICP	0.31
Bi	ICP	<0.05
S	Combustion method	0.47
SiO ₂	Colorimetry	33.00
Magnetite	Satmagan	11.70

an ice-water mixture after annealing the sample at 1250 °C for a certain time. Preliminary experiments indicated that the reduction of copper slag with biochar occurred within 5 min, although it took a longer time for copper slag reduction using fossil coke. Therefore, the experiments with a reduction time of 5 min were only conducted when using biochar.

Analytical Methods

The quenched samples were dried in ambient air and then mounted in epoxy. The cross-sections of the samples were prepared by grinding and polishing using the wet metallographic method. The polished cross-sections were coated with carbon using a carbon evaporator (JEOL IB-29510VET). The microstructures and major compositions were determined using a scanning electron microscope (SEM, Tescan MIRA 3, Brno, Czech Republic) equipped with an UltraDry silicon drift energy-dispersive X-ray spectrometer (EDS, Thermo Fisher Scientific, Waltham, MA, USA).

The elemental concentrations were obtained accurately using a Cameca SX100 electron probe microanalyzer (EPMA, Cameca SAS, Genevilliers, France) with wave dispersive spectroscopy (WDS). An accelerating voltage and beam current of 20 kV and 20 nA, respectively, were employed in the EPMA analyses. Both a focused and a defocused beam diameter set to 5 μm, 10 μm, and 20 μm were used. At least six points were randomly selected from those

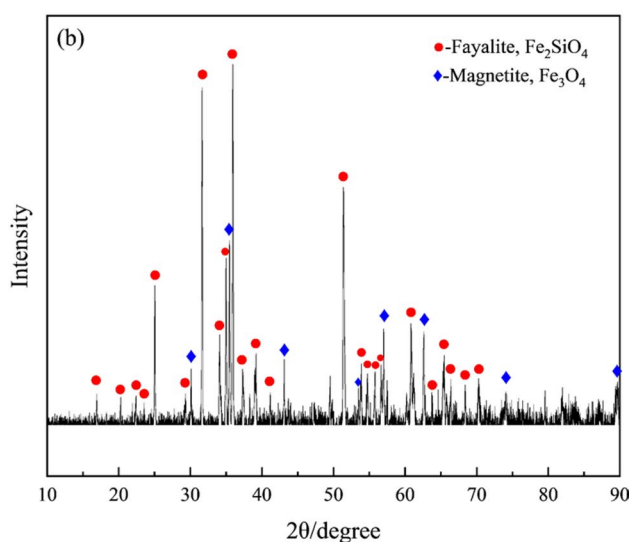
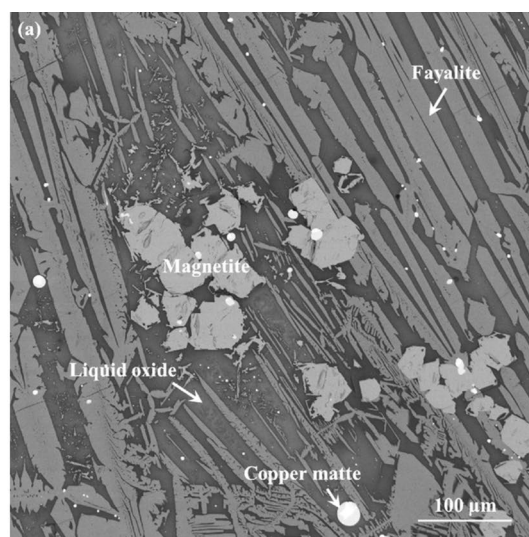


Fig. 2 Representative microstructure (a) and XRD pattern (b) of the industrial copper slag used in this study

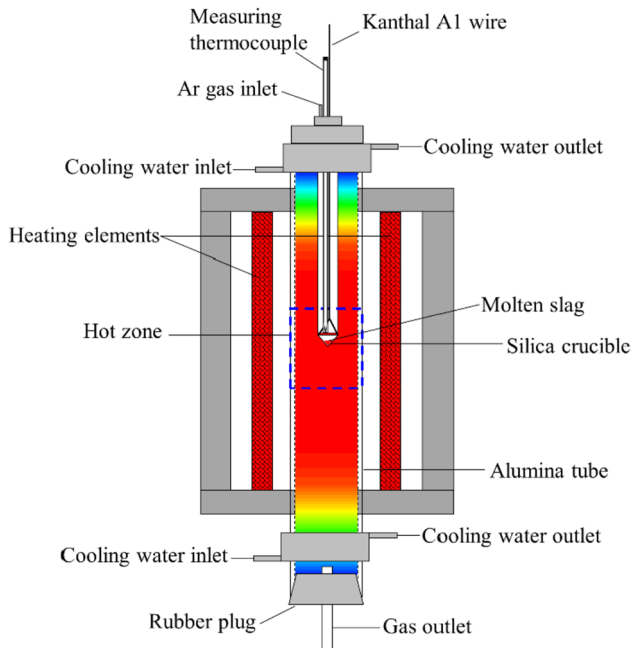
areas without precipitations in each phase. Natural and synthetic minerals and metals were used as standards, as shown in Table 4. The analytical results have been corrected using the PAP online correction program [36].

Results and Discussion

Figure 4 shows the microstructural evolution of the copper alloy and matte as a function of reduction time. The metal-to-matte ratio was increased by extending the reduction time. The increase in the stoichiometric ratio of reductant to slag also led to an increase in the metal-to-matte ratio with the same reduction time. The matte and slag phases were relatively more homogenous than the metal phase due to the segregation of arsenic- and lead-rich phases during

Table 3 Compositions of coke and biochar used in the present study

Reductant	Concentration/wt%				Stoichiometric ratio	
	Carbon	Ash	Volatiles	Moisture	1	2
Coke	86	11–12	< 1	< 1	0.0126 g	0.0253 g
Biochar	90	3	4	–	0.0157 g	0.0315 g

**Fig. 3** Schematic diagram of the experimental setup**Table 4** Average detection limits of EPMA for matte, alloy, and slag phases

Element	Standard	X-ray line	Detection limits of EPMA/ppm		
			Slag	Matte	Metal
O	Obsidian	K α	2437	1450	1183
Si	Quartz	K α	272	288	355
Al	Almandine	K α	241	330	387
Mg	Diopside	K α	297	446	492
K	Sanidine	K α	126	148	153
Fe	Hematite	K α	259	249	262
Co	Metal	K α	333	266	282
As	GaAs	K α	2995	3581	3836
Bi	BiSe	L α	2399	2840	3131
Ni	Metal	K α	300	341	371
Cu	Metal	K α	347	480	481
Zn	Sphalerite	K α	411	523	519
Ca	Diopside	K α	117	139	–
S	Sphalerite	K α	156	198	206
Sb	Sb ₂ Te ₃	L α	405	467	566
Pb	Galena	M α	497	821	654
Na	Tugtupite	K α	360	344	–

quenching. After reduction, no solid phases were observed in the quenched molten slag, indicating that most of the magnetite had reduced to ferrous oxide and dissolved in the slag.

Concentrations of Metals in the Alloy

Figure 5 shows the concentrations of various metal elements in the alloy phase determined by EPMA. The copper concentrations in the metallic copper alloy increased from approximately 50 wt% to 70 wt% when extending the reduction time, as shown in Fig. 5a. Biochar and coke had almost the same reduction effect on the copper concentration in the copper alloy. However, the amount of coke and biochar had no appreciable influence on the copper concentration in the copper alloy. To investigate the effect of the initial slag amount on the reduction, an experiment with 3 g of copper slag and one stoichiometric amount of coke was conducted. The initial slag amount used for the experiment had no obvious effect on the copper concentration in the copper alloy, similarly to the results for other elements in the copper alloy investigated in this study.

The concentrations of iron in the copper alloy displayed different trends against reduction time, as shown in Fig. 5b. As for the samples reduced by one stoichiometric amount of coke, the iron concentration of the copper alloy remained almost constant at approximately 1.6 wt% over the entire reduction range investigated in this study. The increase of the stoichiometric ratio of coke from one to two led to a small increase of iron in the copper alloy at a given reduction time. However, the iron concentration in the copper alloy obtained using one stoichiometric amount of biochar increased when extending the reduction time. By increasing the stoichiometric ratio of biochar from one to two, the iron concentration in the copper alloy increased from approximately 3 wt% to 7 wt%, which was much higher than that obtained using the stoichiometric ratio of biochar of one, indicating that biochar is a much stronger reductant than coke.

Figure 5c indicates that the nickel concentration in the copper alloy decreased from approximately 12 wt% to 5 wt% when extending the reduction time, regardless of the type and amount of reductant used for the experiments. The concentration of cobalt in the copper alloy displayed similar trends to iron as a function of reduction time, as shown in Fig. 5d. However, the results for cobalt were lower than those for iron, varying between approximately 0.2 wt% and

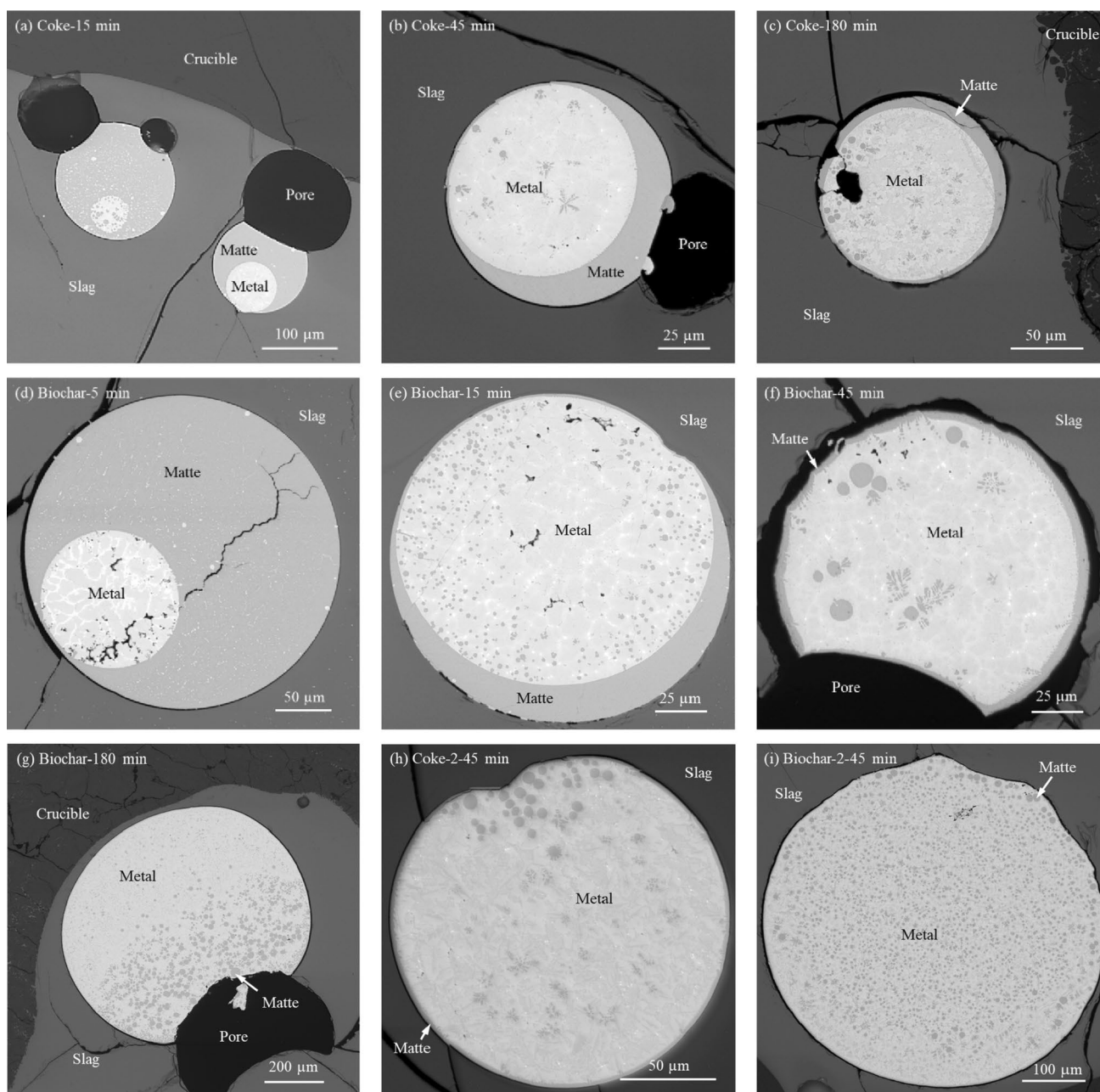


Fig. 4 Microstructural evolution of copper alloy and matte versus reduction time after quenching; **a–c** coke with stoichiometric ratio of 1; **d–g** biochar with stoichiometric ratio of 1; **h** coke with stoichiometric ratio of 2; **i** biochar with stoichiometric ratio of 2

0.6 wt%. Biochar was more effective in reducing cobalt into the copper alloy. The increase of the amount of biochar and coke also led to an increased cobalt concentration in the copper alloy.

The lead concentration in the copper alloy shown in Fig. 5e varies between approximately 0 and 1 wt% against reduction time. Biochar seems to have a better impact than coke on reducing lead into the copper alloy. The results for antimony in the copper alloy were also scattered, fluctuating between approximately 6 wt% and 16 wt%. The effect

of the type of reductant was not obvious in this study, similarly to that for arsenic in copper alloy.

The results for antimony in Fig. 5f show that the concentration of antimony increased when extending the reduction time. With one stoichiometric amount of reductant, the results obtained using biochar and coke were close at the fixed reduction time. The increase of the stoichiometric ratio of reductant favored the reduction of antimony into the copper alloy phase.

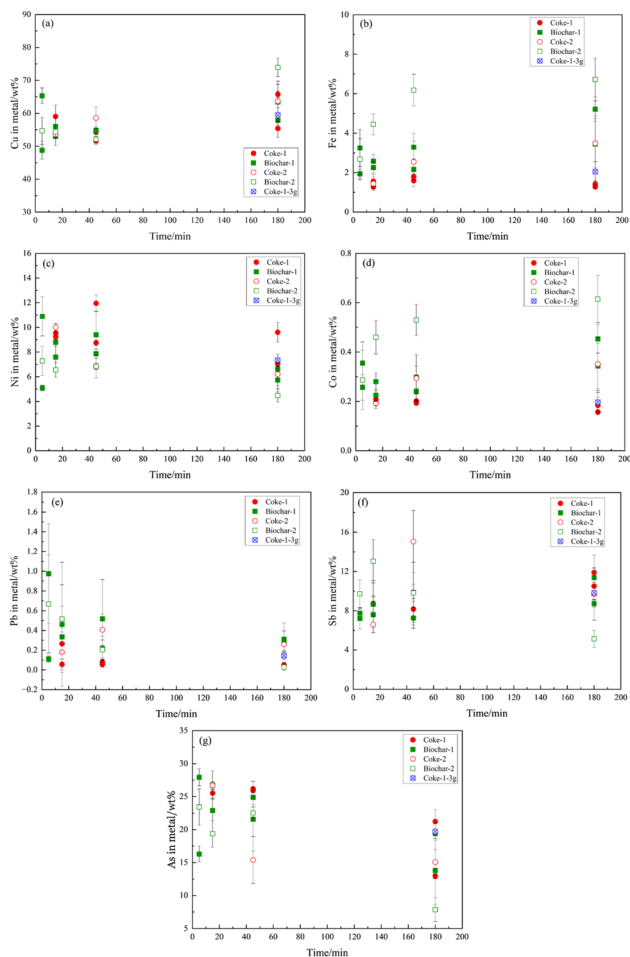


Fig. 5 Concentrations of Cu (a), Fe (b), Ni (c), Co (d), Pb (e), Sb (f) and As (g) in the metal phase as a function of reduction time at 1250 °C for different reductants used in this study

Arsenic was highly enriched into the copper alloy, ranging from approximately 10–27 wt%, as shown in Fig. 5g. The concentration of arsenic in the copper alloy decreased when extending the time, regardless of the type of reductant. The decreasing trend can be ascribed to the volatilization of arsenic into the gas phase. The concentration of zinc in the metal phase was lower than the detection limit of EPMA (about 520 ppm).

Concentrations of Metals in Matte

Figure 6 shows the concentrations of various elements in matte as a function of reduction time. The concentration of copper in matte in Fig. 6a obtained using coke and biochar displays a decreasing trend with reduction time. The results obtained using biochar were lower than those obtained using coke. The increase in the stoichiometric amount of reductant led to a decrease of copper in matte at a given reduction time. The initial amount of slag had no obvious effect on

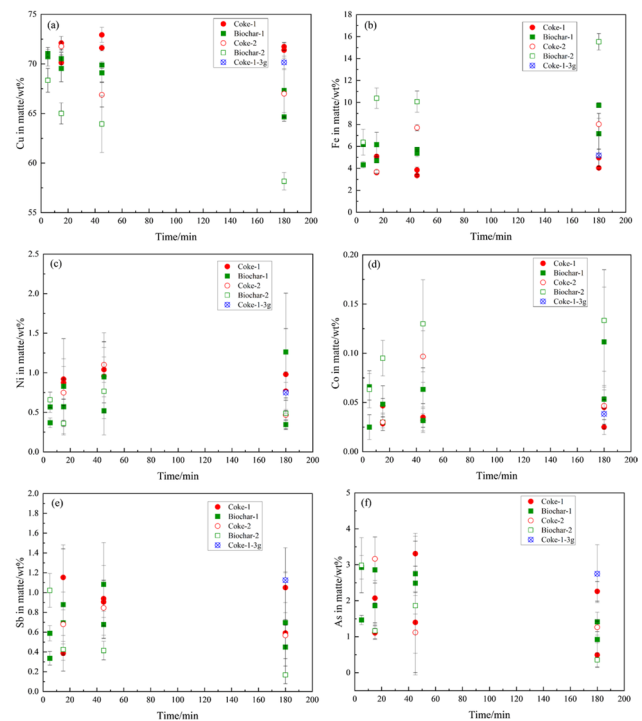


Fig. 6 Concentrations of Cu (a), Fe (b), Ni (c), Co (d), Sb (e) and As (f) in the matte phase as a function of reduction time

the copper concentration in matte, similarly to that of iron, nickel, cobalt, antimony, and arsenic in matte.

In contrast to the concentration of copper in matte, the concentration of iron in matte, shown in Fig. 6b, increased when extending the reduction time. The iron concentration in matte obtained using biochar was higher than that using coke with the stoichiometric amount. The increase of the stoichiometric ratio of reductant from one to two contributed to the increase of iron in matte. The results for nickel and cobalt in matte, as shown in Fig. 6c and d, respectively, displayed similar increasing trends as for iron in matte. However, the results for cobalt were much lower than those for iron and nickel. As for nickel in matte, the use of coke seems to favor its department to matte. Biochar favored the department of cobalt to matte and the use of two stoichiometric amount of reductant increased the cobalt concentration in matte.

The concentrations for antimony in matte shown in Fig. 6e are scattered, varying between approximately 0.2 wt% and 1.2 wt%. The effect of the type of reductant on antimony in matte was not clear in this study. The concentration of arsenic in matte in Fig. 6f determined in this study decreased when extending the reduction time. Similarly to the results for antimony, the scatter of the results led to difficulties in analyzing the effect of the type of reductant. The concentration of zinc in matte was too low to be detected by EPMA.

Concentrations of Metals in Slag

The concentrations of various elements in the reduced copper slag against reduction time are plotted in Fig. 7. Figure 7a indicates that the copper concentration in slag can be reduced to approximately 0.4 wt% to 0.6 wt% within 5 min. A longer reduction time was beneficial for the reduction of copper from the slag. Compared with coke, the reduction behavior for copper in slag using biochar was better, since the copper concentrations in the biochar-reduced slag were on the lower side of the results obtained using coke. The copper concentration in slag decreased with an increasing amount of reductant. It has been reported in the literature [33, 34, 37–40] that the copper concentration in iron silicate slags can be reduced by adding basic oxides such as Al_2O_3 , MgO , and CaO into the slags. The basic oxides in iron silicate slags also break the polymeric silicate network, resulting in a decrease in slag viscosity and physical copper loss in slags. In effect,

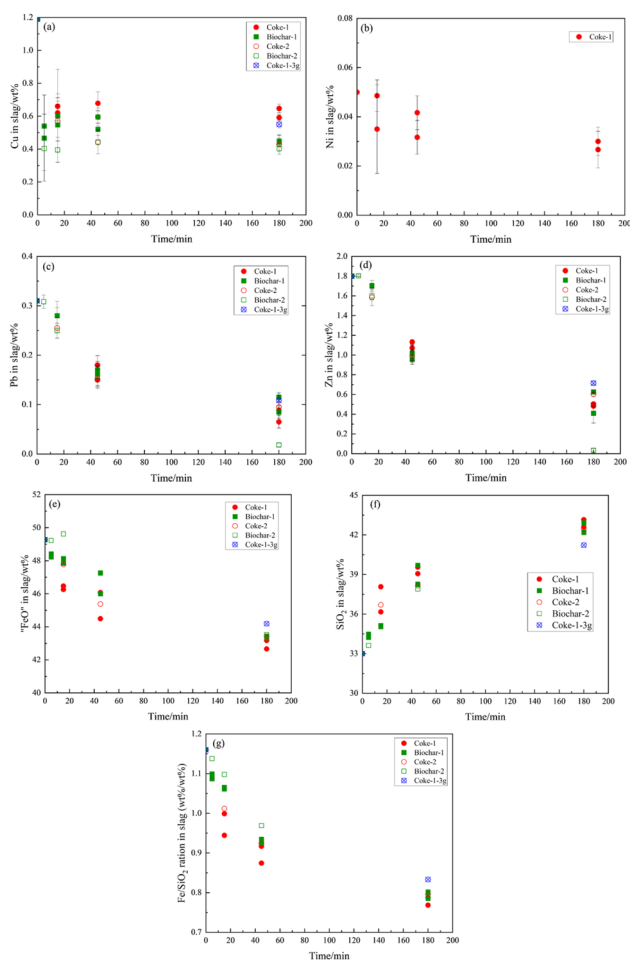


Fig. 7 Concentrations of **a** Cu, **b** Ni, **c** Pb, **d** Zn, **e** “FeO”, **f** SiO_2 and **g** Fe/SiO_2 ratio in the reduced copper slag as a function of the reduction time at 1250 °C in silica crucibles

Al^{3+} , Ca^{2+} , and Mg^{2+} cations replace the copper cations in the silicate network, which leads to a decrease in chemical copper dissolution in slag. The variation of the metal concentrations in the slag in the present study was affected by three types of reactions in the slag. The first was the reduction of ferric oxide to ferrous, which decreased the mass and thus increased the concentrations of other oxides in the initial stage. The second was the dissolution of silica from the crucible, which diluted the oxides. The third was the actual reduction of copper and other oxides to matte and metal.

The nickel concentration in the slag shown in Fig. 7b obtained with one stoichiometric amount of coke decreased when extending the reduction time. The nickel concentration in slag reduced by biochar was lower than the detection limit (about 300 ppm) of EPMA, indicating that biochar worked better than coke for the reduction of nickel.

The concentrations of lead and zinc in slag displayed a similar nonlinear decreasing trend curve against reduction time, as shown in Fig. 7c and d, respectively. The decreasing trend became less steep after 40 min of reduction time. The concentrations of lead and zinc in slag went down to approximately 0.1 wt% and 0.5 wt%, respectively, after being reduced for 180 min. The type and total amount of the reductant had no significant effect on the lead and zinc concentrations in slag.

The concentrations of “FeO”, SiO_2 , and the corresponding Fe/SiO_2 ratio in the slag are shown in Fig. 7e–g, respectively. The iron concentration in the slag was calculated as “FeO” for ease of presentation [41, 42]. Regarding the “FeO” concentration in the reduced copper slag, it displayed a nonlinear decreasing trend against reduction time, which was attributed to the reduction of magnetite. The concentration of silica in the reduced slag showed the opposite increasing trend when extending the reaction time. The dissolution of the silica crucible into the copper slag together with the reduction of ferric oxide are the reasons for the increased silica concentration in the slag and also for the decrease of the Fe/SiO_2 ratio in the slag, as shown in Fig. 7g. The results for the Fe/SiO_2 ratio in the slag reduced by biochar was on the higher side of the data obtained using coke. The Fe/SiO_2 ratios in the slag that was reduced by twice the stoichiometric amounts of coke and biochar were slightly higher than those obtained with the stoichiometric amount of reductant.

The increase of silica concentration shown in Fig. 7f suggests that the dilution effect of silica is about 10% at the endpoints of reduction. This means that the concentrations of the reducible elements would be about 10% higher than the experimental values in Fig. 7.

Distribution of Elements Between Copper Alloy and Slag

The elemental distribution behavior in copper slag reduction can be determined using the distribution coefficients between phases. The logarithmic distribution coefficients of an element Me between e.g., metal and slag, can be calculated based on the following Eq. (10):

$$\text{Log}_{10}L^{\text{Metal/Slag}}(Me) = \text{Log}_{10}\left\{\frac{[Me]_{\text{in metal}}}{(Me)_{\text{in slag}}}\right\} \quad (10)$$

where $[Me]_{\text{in metal}}$ and $(Me)_{\text{in slag}}$ refer to the elemental concentrations of Me in metal and slag, respectively. The calculated logarithmic distribution coefficients of copper, nickel, and lead are shown in Fig. 8. As for other metals, the distribution coefficients could not be determined accurately based on the present EPMA results due to their concentrations in metal or slag being lower than the EPMA detection limits. However, because of the lack of EPMA data for nickel but simultaneously its importance for this study, it was decided to calculate the distribution coefficient for nickel using the detection limit of EPMA. We are aware of the problem that such calculated distribution coefficients based on detection limits represent at best the minimal distribution results into the metal phase and that they are only qualitative. The true nickel concentration in slag may be orders of magnitude smaller than the detection limits, thus the interpretation derived from them is purely speculative; even the opposite case could be possible. Further studies regarding the distribution of nickel need to be carried out in order to obtain the true nickel concentrations in the phases, probably by using the laser ablation-inductively coupled plasma-mass spectrometry technique, which has lower detection limits than EPMA.

The kinetic behavior of slag cleaning was evaluated based on the distribution coefficients and a comparison of the different reductants was made on the same basis. Figure 8a shows that copper can be effectively reduced to copper alloy. The use of biochar and the increase in the amount of reductant for the reduction experiments favored the recovery of copper into the copper alloy phase, although the effects were minor. The distribution of copper between copper alloy and slag was independent of the initial amount of slag used for the reduction experiments, as for nickel and lead. Similarly to the behavior of copper, nickel was recovered to a high degree into the metallic copper alloy phase, as shown in Fig. 8b. When coke was used as reductant, the increase in the stoichiometric amount led to an increase in the distribution coefficient of nickel between the copper alloy and slag. However, the increase of the stoichiometric amount of biochar had an opposite impact from coke on the distribution of nickel between metal and slag.

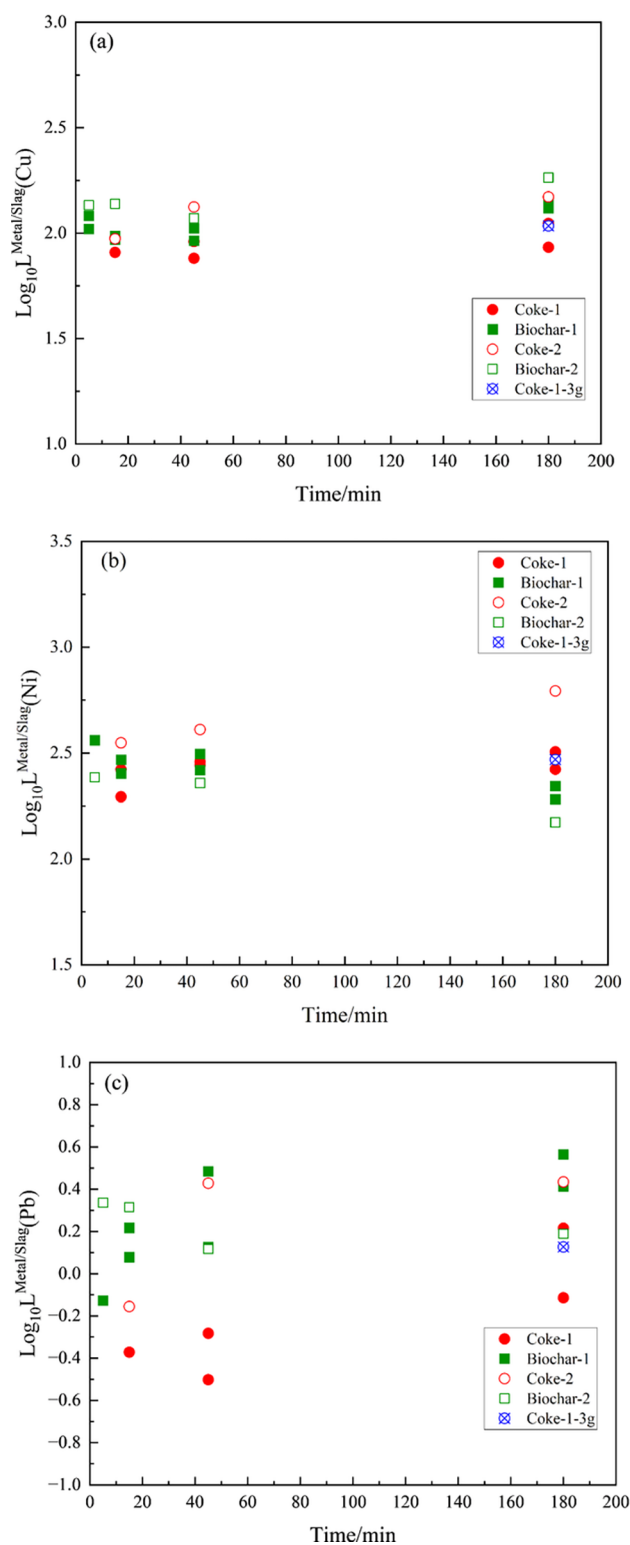


Fig. 8 Development of logarithmic distribution coefficients of Cu (a), Ni (b) and Pb (c) between copper alloy and slag during carbon reduction with different reductants and stoichiometric C/slag ratios at 1250 °C

Figure 8c indicates that the distribution of lead between copper alloy and slag was highly dependent on the type of reductant used. Lead could not be effectively recovered into the metal phase when one stoichiometric amount of coke was used, since the logarithmic distribution coefficient was lower than zero. However, the use of twice the stoichiometric amount of coke favored the recovery of lead from slag to the metal phase and the distribution coefficient displayed an increasing trend as a function of reduction time. Biochar worked better than coke in recovering lead into the copper alloy phase and the recovery rate of lead by biochar increased when extending the reduction time, whereas the opposite trend was obtained for the stoichiometric amount of coke.

Distributions of Elements Between Copper Matte and Slag

The distribution coefficients of copper and nickel between matte and slag displayed in Fig. 9 were calculated from the EPMA data. The distribution coefficients for other elements were not calculated because their concentrations either in the matte or slag were too low to be detected reliably by EPMA.

Figure 9a shows that, compared with the slag phase, copper was preferentially enriched in the matte phase. Biochar had a stronger impact than coke on enriching copper into matte from slag. The higher amount of reductant used for the copper slag reduction in this study favored the incorporation of copper into matte rather than slag. The distribution of nickel between matte and slag, as shown in Fig. 9b, indicates that nickel preferentially departed to matte rather than slag. The distribution results for nickel increased when extending the reduction time and when increasing the stoichiometric amount of reductant. The initial slag amount used for the experiments had little effect on the distribution of copper and nickel between matte and slag, indicating a modest scale independence of the present experimental technique.

Distributions of Elements Between Copper Alloy and Matte

Figure 10 shows the logarithmic distribution coefficients of various metals between copper alloy and matte. The distribution of copper into the copper alloy increased slightly with extended reduction time, as shown in Fig. 10a. The fast reduction kinetics of antimony and arsenic from the slag and their department to the alloy was also evident. The type of reductant and the amount of the total reductant used had no evident effect on the distribution of copper between copper alloy and matte.

Figure 10b indicates that iron was preferentially incorporated into matte rather than copper alloy. Biochar favored the distribution of iron into copper alloy rather than matte

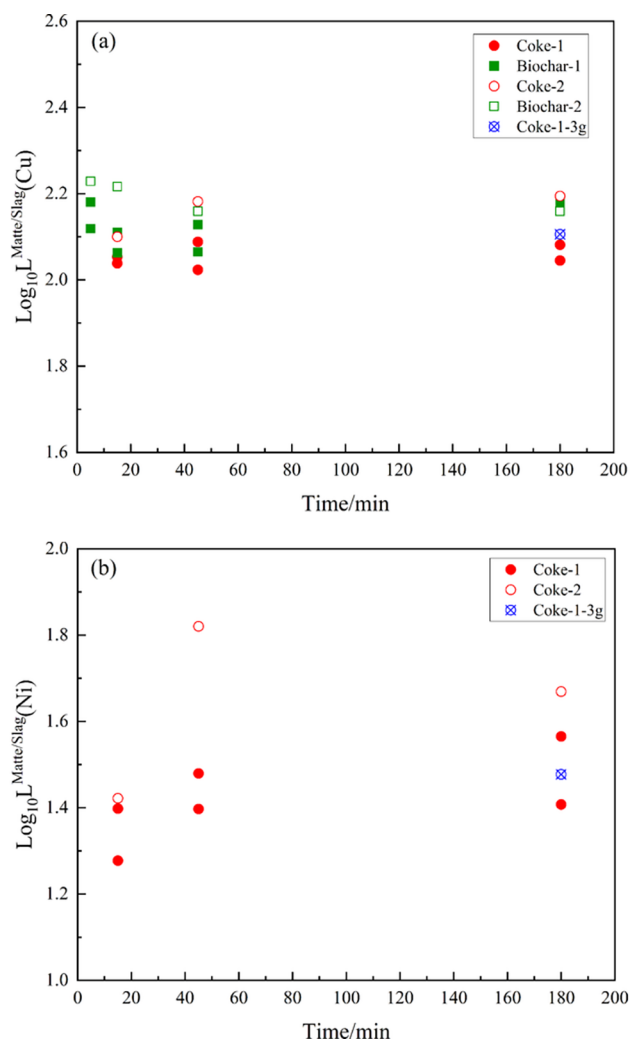


Fig. 9 Development of logarithmic distribution coefficients of copper (a) and nickel (b) between copper matte and slag during carbon reduction of an industrial copper smelting slag at 1250 °C

when compared with coke. The use of two stoichiometric amounts of reductant had little effect on the distribution of iron between copper alloy and slag. The logarithmic distribution coefficient of nickel between copper alloy and matte, as shown in Fig. 10c, displayed a decreasing trend with an extended the reduction time, independent of the type of reductant. Compared with the matte phase, nickel was preferentially enriched in the copper alloy phase. The effect of the type of reductant used in this study was not very clear due to the scatter of the results, which is the same case for cobalt, antimony, and arsenic.

Figure 10d shows that the logarithmic distribution of cobalt between copper alloy and matte decreased slightly with extended reduction time, varying between approximately 0.4 and 1.0. The distribution of antimony and arsenic between copper alloy and matte, as shown in Fig. 10e–f, respectively, displayed similar trend as a function of

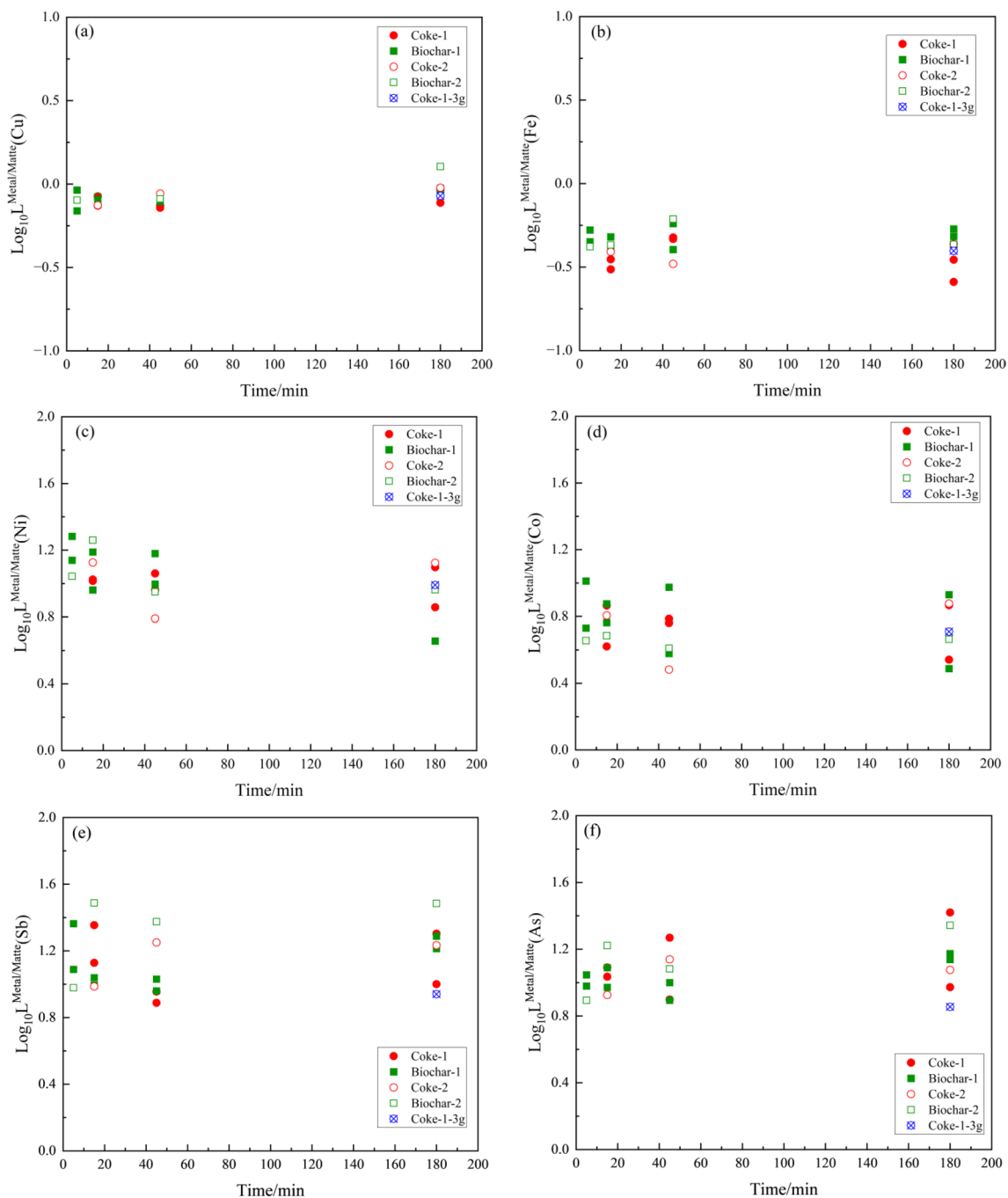


Fig. 10 Development of logarithmic distribution coefficients of copper (a), iron (b), nickel (c), cobalt (d), antimony (e) and arsenic (f) between copper alloy and matte during carbon reduction of an industrial copper smelting slag at 1250 °C

reduction time. Their logarithmic distribution coefficients between copper alloy and matte fluctuated between approximately 0.8 and 1.4, indicating that antimony and arsenic are preferentially deposited to the copper alloy rather than the matte.

The distribution kinetics of copper and the trace elements show only minor variation as a function of reduction time. Nevertheless, there is a general trend of an increasing

distribution coefficient as a function of time. Notably, substantial differences exist among various reductants, especially in the case of cobalt and nickel oxides, which undergo only slight reduction prior to iron. Although EPMA analyses were conducted on numerous alloy droplets in each sample, helping to mitigate variations, the scatter across different samples within the experimental series remained considerable.

Conclusions

The high-temperature isothermal reduction kinetics of copper slag using coke and biochar was investigated by a drop quenching technique using different contact times. The experiments were conducted at 1250 °C in silica crucibles under a flowing Ar gas atmosphere. The direct phase composition analyses were made using EPMA. The effects of time and the amount of reductant on the copper slag cleaning were investigated in this study and a large variation was found in the deportment of elements in the case of cobalt, nickel and iron, depending on the type of reductant.

The matte mostly originated from physically entrained droplets in the initial slag. The copper concentration in metal was found to increase when extending the reaction time when copper was depleted from the slag. An increase in the stoichiometric amount of coke and biochar led to an increase of iron and copper in the metal alloy. However, the nickel and arsenic in the metal alloy displayed the opposite downward trend. The concentrations of copper and arsenic in the matte decreased when extending the reaction time. The increase in the stoichiometric amount of coke and biochar led to an increase of iron in the matte although, due to the high matte-to-metal distribution coefficient [43], the corresponding increase of iron in the metal alloy was within the experimental scatter of EPMA. The concentrations of nickel, lead, zinc, “FeO”, and the Fe/SiO₂ ratio in slag decreased with extended reaction time, showing the progress of reduction in the slag and dissolution of the silica crucible.

The reduction kinetics were evaluated based on the matte/metal-to-slag distribution coefficients. The present study shows that copper concentration in the slag can be reduced to 0.4–0.6 wt% (Cu) within a short reduction time. Generally, biochar exhibited kinetically superior behavior in the reduction of metals from slag, as indicated by the large variations in the distribution coefficients of the trace elements and iron. Copper and nickel can be effectively recovered into the metal phase. In addition, antimony and arsenic were effectively dissolved in the alloy. The use of biochar also favored the deportment of lead to the metal phase. A significant amount of zinc deported to the gas phase. The distribution coefficients of the trace elements were found not to be particularly dependent on time.

Supplementary Information The online version contains supplementary material available at <https://doi.org/10.1007/s40831-024-00793-7>.

Acknowledgements This study used the Academy of Finland’s Raw-MatTERS Finland Infrastructure (RAMI) based at Aalto University, GTK, Espoo, and VTT Espoo.

Author Contributions MC: Conceptualization, Investigation, Methodology, Software, Data curation, Writing-original draft. DS: Methodology, Supervision, Validation, Writing-review and editing. PT: Methodology, Software, Supervision, Validation, Writing-review and editing.

JH: Writing-review and editing. RMM: Writing-review and editing. ML: Writing-review and editing. AJ: Supervision, Project administration, Resources, Validation, Funding acquisition, Writing-review and editing.

Funding Open Access funding provided by Aalto University.

Declarations

Conflicts of interest The author declares no conflict of interest.

Open Access This article is licensed under a Creative Commons Attribution 4.0 International License, which permits use, sharing, adaptation, distribution and reproduction in any medium or format, as long as you give appropriate credit to the original author(s) and the source, provide a link to the Creative Commons licence, and indicate if changes were made. The images or other third party material in this article are included in the article’s Creative Commons licence, unless indicated otherwise in a credit line to the material. If material is not included in the article’s Creative Commons licence and your intended use is not permitted by statutory regulation or exceeds the permitted use, you will need to obtain permission directly from the copyright holder. To view a copy of this licence, visit <http://creativecommons.org/licenses/by/4.0/>.

References

- Klaffenbach E, Montenegro V, Guo M, Blanpain B (2023) Sustainable and comprehensive utilization of copper slag: a review and critical analysis. *J Sustain Metall* 9:468–496. <https://doi.org/10.1007/s40831-023-00683-4>
- Chen M, Avarmaa K, Klemettinen L, O’Brien H, Sukhomlinov D, Shi J, Taskinen P, Jokilaakso A (2020) Recovery of precious metals (Au, Ag, Pt, and Pd) from urban mining through copper smelting. *Metall Mater Trans B* 51(4):1495–1508. <https://doi.org/10.1007/s11663-020-01861-5>
- Shuva MAH, Rhamdhani MA, Brooks GA, Masood S, Reuter MA (2016) Thermodynamics data of valuable elements relevant to e-waste processing through primary and secondary copper production: a review. *J Clean Prod* 131:795–809. <https://doi.org/10.1016/j.jclepro.2016.04.061>
- Reuter MA, Kojo IV (2014) Copper: a key enabler of resource efficiency. *World Metall Erzmetall* 67(1):5–12
- Shen H, Forssberg E (2003) An overview of recovery of metals from slags. *Waste Manage* 23(10):933–949. [https://doi.org/10.1016/S0956-053X\(02\)00164-2](https://doi.org/10.1016/S0956-053X(02)00164-2)
- Zhang L, Zhou H, Chen X, Liu G, Jiang C, Zheng L (2021) Study of the micromorphology and health risks of arsenic in copper smelting slag tailings for safe resource utilization. *Ecotoxicol Environ Saf* 219:112321. <https://doi.org/10.1016/j.ecoenv.2021.112321>
- Gorai B, Jana RK (2003) Characteristics and utilisation of copper slag—a review. *Resour Conserv Recycl* 39(4):299–313. [https://doi.org/10.1016/S0921-3449\(02\)00171-4](https://doi.org/10.1016/S0921-3449(02)00171-4)
- Qu G, Wei Y, Li B, Wang H, Yang Y, McLean A (2020) Distribution of copper and iron components with hydrogen reduction of copper slag. *J Alloy Compd* 824:153910. <https://doi.org/10.1016/j.jallcom.2020.153910>
- Sarfo P, Das A, Wyss G, Young C (2017) Recovery of metal values from copper slag and reuse of residual secondary slag. *Waste Manage* 70:272–281. <https://doi.org/10.1016/j.wasman.2017.09.024>

10. Shi C, Meyer C, Behnood A (2008) Utilization of copper slag in cement and concrete. *Resour Conserv Recycl* 52(10):1115–1120. <https://doi.org/10.1016/j.resconrec.2008.06.008>
11. Zhou S, Wei Y, Li B, Wang H (2019) Cleaner recycling of iron from waste copper slag by using walnut shell char as green reductant. *J Clean Prod* 217:423–431. <https://doi.org/10.1016/j.jclepro.2019.01.184>
12. Zhou S, Wei Y, Zhang S, Li B, Wang H, Yang Y, Barati M (2019) Reduction of copper smelting slag using waste cooking oil. *J Clean Prod* 236:117668. <https://doi.org/10.1016/j.jclepro.2019.117668>
13. Piri TC, Singh P, Nikoloski N (2021) The potential for copper slag waste as a resource for a circular economy: a review-Part II. *Miner Eng* 172:107150. <https://doi.org/10.1016/j.mineng.2021.107150>
14. Cao B, Wang N, Chen M (2022) Comprehensive recovery of multisource metallurgical solid wastes: Coupling modification and carbothermic reduction of converter slag and copper Slag. In: Peng Z et al (eds) 12th international symposium on high-temperature metallurgical processing. Springer, Cham, pp 469–479
15. Guo Z, Zhu D, Pan J, Yao W, Xu W, Chen J (2017) Effect of Na_2CO_3 addition on carbothermic reduction of copper smelting slag to prepare crude Fe-Cu alloy. *JOM* 69:1688–1695. <https://doi.org/10.1007/s11837-017-2410-y>
16. Guo Z, Zhu D, Pan J, Zhang F (2018) Innovative methodology for comprehensive and harmless utilization of waste copper slag via selective reduction-magnetic separation process. *J Clean Prod* 187:910–922. <https://doi.org/10.1016/j.jclepro.2018.03.264>
17. Heo JH, Kim BS, Park JH (2013) Effect of CaO addition on iron recovery from copper smelting slags by solid carbon. *Metall Mater Trans B* 44:1352–1363. <https://doi.org/10.1007/s11663-013-9908-7>
18. Li L, Wang H (2015) Response characteristics of iron smelting reduction of copper slags. *Mater Res Innov* 19:469–473. <https://doi.org/10.1179/1432891714Z.0000000001133>
19. Li S, Pan J, Zhu D, Guo Z, Xu J, Chou J (2019) A novel process to upgrade the copper slag by direct reduction-magnetic separation with the addition of Na_2CO_3 and CaO. *Powder Technol* 347:159–169. <https://doi.org/10.1016/j.powtec.2019.02.046>
20. Long H, Meng Q, Chun T, Wang P, Li J (2016) Preparation of metallic iron powder from copper slag by carbothermic reduction and magnetic separation. *Can Metall Q* 55(3):338–344. <https://doi.org/10.1080/00084433.2016.1181313>
21. Yücel O, Sahin F, Sirin B, Addeemir O (1999) A reduction study of copper slag in a DC arc furnace. *Scand J Metall* 28(3):93–99
22. Zhai Q, Liu R, Wang C, Wen X, Li X, Sun W (2022) A novel scheme for the utilization of Cu slag flotation tailings in preparing internal electrolysis materials to degrade printing and dyeing wastewater. *J Hazard Mater* 424:127537. <https://doi.org/10.1016/j.jhazmat.2021.127537>
23. Zuo Z, Yu Q, Wei M, Xie H, Duan W, Wang K, Qin Q (2016) Thermogravimetric study of the reduction of copper slag by biomass: reduction characteristics and kinetics. *J Therm Anal Calorim* 126:481–491. <https://doi.org/10.1007/s10973-016-5570-z>
24. Yuan P, Shen B, Duan D, Adwek G, Mei X, Lu F (2017) Study on the formation of direct reduced iron by using biomass as reductants of carbon containing pellets in RHF process. *Energy* 141:472–482. <https://doi.org/10.1016/j.energy.2017.09.058>
25. Wang JP, Erdenebold U (2020) A study on reduction of copper smelting slag by carbon for recycling into metal values and cement raw material. *Sustainability* 12(4):1421. <https://doi.org/10.3390/su12041421>
26. Wei Y, Zhang T, Li B, Zhou S (2020) Copper smelting slag cleaning in an electric furnace by using waste cooking oil. *Metall Mater Trans B* 51:2756–2768. <https://doi.org/10.1007/s11663-020-01986-7>
27. Zhu D, Xu J, Guo Z, Pan J, Li S, Pan L, Yang C (2020) Synergetic utilization of copper slag and ferruginous manganese ore via co-reduction followed by magnetic separation process. *J Clean Prod* 250:119462. <https://doi.org/10.1016/j.jclepro.2019.119462>
28. Lan C, Zhang S, Liu R, Lyu Q, Yan G, Wang B (2022) Thermodynamic and kinetic behaviours of copper slag carbothermic reduction process. *Ironmaking Steelmaking* 50(2):123–133. <https://doi.org/10.1080/03019233.2022.2091726>
29. Tang Z, Yu W, Wu W, Zhu L, Ye Y, Gao C, Wang B, Ren S (2023) Preparation of Fe-Cu bimetal from copper slag by carbothermic reduction-magnetic process for activating persulfate to degrade bisphenol A. *J Taiwan Inst Chem Eng* 146:104784. <https://doi.org/10.1016/j.jtice.2023.104784>
30. Avarmaa K, Järvenpää M, Klemettinen L, Marjakoski M, Taskinen P, Lindberg D, Jokilaakso A (2020) Battery scrap and biochar utilization for improved metal recoveries in nickel slag cleaning conditions. *Batteries* 6(4):58. <https://doi.org/10.3390/batteries6040058>
31. Avarmaa K, Taskinen P, Klemettinen L, O'Brien H, Lindberg D (2021) Ni-Fe-Co alloy-magnesia-iron-silicate slag equilibria and the behavior of minor elements Cu and P in nickel slag cleaning. *J Market Res* 15:719–730. <https://doi.org/10.1016/j.jmrt.2021.07.112>
32. Gisby J, Taskinen P, Pihlasalo J, Li Z, Tyrer M, Pearce J, Avarmaa K, Björklund P, Davies H, Korpi M, Martin S, Pesonen L, Robinson J (2017) MTDATA and the prediction of phase equilibria in oxide systems: 30 years of industrial collaboration. *Metall Mater Trans B* 48B(1):91–98. <https://doi.org/10.1007/s11663-016-0811-x>
33. Chen M, Avarmaa K, Klemettinen L, Shi J, Taskinen P, Jokilaakso A (2020) Experimental study on the phase equilibrium of copper matte and silica-saturated $\text{FeO}_x\text{-SiO}_2$ -based slags in pyrometallurgical WEEE processing. *Metall Mater Trans B* 51(4):1552–1563. <https://doi.org/10.1007/s11663-020-01874-0>
34. Chen M, Avarmaa K, Klemettinen L, Shi J, Taskinen P, Lindberg D, Jokilaakso A (2020) Equilibrium of copper matte and silica-saturated iron silicate slags at 1300°C and PSO_2 of 05 atm. *Metall Mater Trans B* 51(5):2107–2118. <https://doi.org/10.1007/s11663-020-01933-6>
35. Chen M, Avarmaa K, Klemettinen L, O'Brien H, Shi J, Taskinen P, Lindberg D, Jokilaakso A (2021) Precious metal distributions between copper matte and slag at high P_{SO_2} in WEEE reprocessing. *Metall Mater Trans B* 52(2):871–882. <https://doi.org/10.1007/s11663-021-02059-z>
36. Pouchou J, Pichoir L (1986) Basic expression of “PAP” computation for quantitative EPMA. In: Brown JD, Packwood RH (eds) Proceedings of the 11th international congress on X-ray optics and microanalysis (ICXOM). University of Western Ontario, London, pp 249–256
37. Kim HG, Sohn HY (1998) Effects of CaO, Al_2O_3 , and MgO additions on the copper solubility, ferric/ferrous ratio, and minor-element behavior of iron-silicate slags. *Metall Mater Trans B* 29:583–590. <https://doi.org/10.1007/s11663-998-0093-z>
38. Shishin D, Hidayat T, Fallah-Mehrjardi A, Hayes PC, Decterov SA, Jak E (2019) Integrated experimental and thermodynamic modeling study of the effects of Al_2O_3 , CaO, and MgO on slag-matte equilibria in the Cu-Fe-O-S-Si-(Al, Ca, Mg) system. *J Phase Equilib Diffus* 40:445–461. <https://doi.org/10.1007/s11669-019-00716-0>
39. Sineva S, Shishin D, Shevchenko M, Hayes PC, Jak E (2023) Experimental study of the combined effects of Al_2O_3 , CaO and MgO on gas/slag/matte/spinel equilibria in the Cu-Fe-O-S-Si-Al-Ca-Mg system at 1473 K (1200 °C) and $p(\text{SO}_2) = 025$ atm. *J Sustain Metall* 9(2):599–612

40. Sukhomlinov D, Klemettinen L, O'Brien H, Taskinen P, Jokilaakso A (2019) Behavior of Ga, In, Sn, and Te in copper matte smelting. *Metall Mater Trans B* 50(6):2723–2732. <https://doi.org/10.1007/s11663-019-01693-y>
41. Chen M, Avarmaa K, Taskinen P, Michallik R, Jokilaakso A (2022) An experimental study on the phase equilibria of FeO_x-saturated iron silicate slags and metallic copper alloys at 1200–1300 °C. *Calphad* 77:102418. <https://doi.org/10.1016/j.calphad.2022.102418>
42. Tian M, Wan X, Chen M, Taskinen P, Tiljander M, Jokilaakso A (2022) Phase equilibria of FeO_x-SiO₂-Al₂O₃ slag system at 1200 °C and pO₂ of 10–86 atm. *Calphad* 79:102502. <https://doi.org/10.1016/j.calphad.2022.102502>
43. Coursol P, Cardona Valencia N, Mackey P, Bell S, Davis B (2012) Minimization of copper losses in copper smelting slag during electric furnace treatment. *JOM* 64:1305–1313. <https://doi.org/10.1007/s11837-012-0454-6>

Publisher's Note Springer Nature remains neutral with regard to jurisdictional claims in published maps and institutional affiliations.